Continental Shelf Research 148 (2017) 185–198

Contents lists available at ScienceDirect

Continental Shelf Research

journal homepage: www.elsevier.com/locate/csr

Circulation and water properties in the landfast ice zone of the Alaskan Beaufort Sea

Thomas J. Weingartner[a,*], Seth L. Danielson[a], Rachel A. Potter[a], John H. Trefry[b], Andy Mahoney[c], Mark Savoie[d], Cayman Irvine[a], Leandra Sousa[e]

[a] Institute of Marine Science, University of Alaska, Fairbanks, AK 99775, USA
[b] Florida Institute of Technology, Ocean Engineering and Sciences, 150 W. University Blvd., Melbourne, FL 32901, USA
[c] Geophysical Institute, University of Alaska, Fairbanks, AK 99775, USA
[d] Kinnetic Labs, 704 West 2nd Ave, Anchorage, AK 99501, USA
[e] North Slope Borough, Department of Wildlife Management, P.O. Box 69, Barrow/Utqiaġvik, AK 99723 USA

ARTICLE INFO

Keywords:
Landfast ice zone
Alaskan Beaufort Sea
Nearshore circulation

ABSTRACT

Moorings, hydrography, satellite-tracked drifters, and high-frequency radar data describe the annual cycle in circulation and water properties in the landfast ice zone (LIZ) of the Alaskan Beaufort Sea. Three seasons, whose duration and characteristics are controlled by landfast ice formation and ablation, define the LIZ: "winter", "break-up", and "open-water". Winter begins in October with ice formation and ends in June when rivers commence discharging. Winter LIZ ice velocities are zero, under-ice currents are weak ($\sim$5 cm s^{-1}), and poorly correlated with winds and local sea level. The along-shore momentum balance is between along-shore pressure gradients and bottom and ice-ocean friction. Currents at the landfast ice-edge are swift ($\sim$35 cm s^{-1}), wind-driven, with large horizontal shears, and potentially unstable. Weak cross-shore velocities ($\sim$1 cm s^{-1}) imply limited exchanges between the LIZ and the outer shelf in winter. The month-long break-up season (June) begins with the spring freshet and concludes when landfast ice detaches from the bottom. Cross-shore currents increase, and the LIZ hosts shallow ($\sim$2 m), strongly-stratified, buoyant and sediment-laden, under-ice river plumes that overlie a sharp, $\sim$1 m thick, pycnocline across which salinity increases by $\sim$30. The plume salt balance is between entrainment and cross-shore advection. Break-up is followed by the 3-month long open-water season when currents are swift ($\geq$20 cm s^{-1}) and predominantly wind-driven. Winter water properties are initialized by fall advection and evolve slowly due to salt rejection from ice. Fall waters and ice within the LIZ derive from local rivers, the Mackenzie and/or Chukchi shelves, and the Arctic basin.

1. Introduction

Wind stresses and buoyancy fluxes influence circulation and water property modifications on all continental shelves, particularly over the inner shelf. On arctic shelves, these influences are modulated by the annual freeze/thaw cycle, which controls the phasing and duration of river discharge and landfast ice. Landfast ice becomes bottom-fast in waters shallower than approximately 1.5 m, but typically extends offshore to about the 20 m isobath and is held in place by grounded ridges (Reimnitz, 2000; Mahoney et al., 2007a). Over the broad and gently sloping Eurasian shelf seas the width of the landfast ice zone (LIZ) can be $\sim$100 km (Zubov, 1945; Wadhams, 1986; Morris et al., 1997; Eicken et al., 2005a), while on the narrower Beaufort Sea shelf it is more typically $\sim$20–40 km (Reimnitz and Kempema, 1984; Barnes et al., 1984; Macdonald and Carmack, 1991; Mahoney et al., 2014). Approximately 25% of the Alaskan Beaufort Sea (ABS) shelf is covered by landfast ice for $\sim$9 months (October – June). Landfast ice is effectively immobile and inhibits air-sea heat and momentum transfers while also providing a frictional boundary for the under-ice flow. Consequently, the ice is expected to have an important influence on the circulation characteristics of the inner shelf. For convenience, we refer to the inner shelf as where water depths are $\leq\sim$20 m. This definition differs from one defined by dynamic processes; i.e., that portion of the shelf over which the surface and bottom boundary layers overlap (Lentz, 1995; Li and Weisberg, 1999). A dynamically-based definition is difficult to apply in landfast ice regions where the surface and bottom boundary layers appear thin (Kasper and Weingartner, 2012) and where there is extreme seasonality in the circulation characteristics.

Frictional coupling between landfast ice and the ocean is poorly understood because it depends on the under-ice topography and current

* Corresponding author.
E-mail address: tjweingartner@alaska.edu (T.J. Weingartner).

http://dx.doi.org/10.1016/j.csr.2017.09.001
Received 23 March 2017; Received in revised form 30 August 2017; Accepted 1 September 2017
Available online 05 September 2017
0278-4343/

speed, both of which may vary considerably with space and time (Shirasawa and Ingram, 1997; McPhee, 1990; Lu et al., 2011). For example, on windward shelves, such as the ABS, the seaward boundary of the LIZ is highly deformed due to collisions with the mobile pack ice. Deformation is an integral part of the seasonal development of the LIZ (Mahoney et al., 2007a). Ridging intensity and keel depths vary alongshore and generally increase offshore and through the freezing season (Tucker et al., 1979). Ice keels can gouge the seafloor (Barnes et al., 1984) and form grounded, rubbled ice, or stamukhi (Zubov, 1945), within and at the edge of the LIZ. The stamukhi protects the inner shelf from pack ice (Reimnitz and Kempena, 1984), inhibits water exchange between the inner and outer portion of the shelf (Macdonald and Carmack, 1991), and, under appropriate wind conditions, may be bounded offshore by a flaw lead wherein new ice rapidly forms (Melling, 1993; Dmitrenko et al., 2005; Itkin et al., 2015). In addition to the seasonal changes in the LIZ, processes influencing deformation (including landfast ice breakout events) can occur on time scales of hours to days and spatial scales of a few to hundreds of kilometers (Overland and Pease, 1984; Eicken et al., 2011).

The LIZ is an important sub-region of the Arctic Ocean because it is the initial processing site for the freshwater and the dissolved and particulate loads discharged by the massive rivers emptying into the Arctic Ocean. As such the LIZ serves as the Arctic's "estuary" (Macdonald and Carmack, 1991; McClelland et al., 2012; Itkin et al., 2015). It also supports a unique biological habitat (Dunton et al., 2012, 2006), is critical to subsistence cultures, and is the site of marine industrial activities. At present, little is known about LIZ circulation processes, but a warming Arctic, and attendant changes, will affect the LIZ. Although the work reported herein was motivated to guide potential oil spill responses within the LIZ of the ABS, our measurements shed light on physical processes not only within the ABS LIZ, but perhaps on other arctic shelves as well.

Few moored measurements have been made within the LIZ because of ice risks to shallow moorings. We know of only two reported wintertime current measurements from within the LIZ of the ABS and the results are contradictory. Aagaard (1984) concluded that current speeds within the LIZ seldom exceed 10 cm-s^{-1}, whereas Matthews (1981) argued from continuity considerations that speeds of up to 35 cm-s^{-1} might occur occasionally. Both conclusions were tentative because they were based on short duration measurements from instruments moored close to the seabed.

Our measurements were made primarily in the vicinity of Prudhoe Bay, about midway along the ABS coast (with additional moorings in Smith and Camden Bays; Fig. 1a). The ABS shelf is ~80 km wide and extends ~600 km eastward from Barrow to the Mackenzie shelf. The bottom grades smoothly from the coast toward the shelfbreak with a bottom slope of $\sim 8 \times 10^{-4}$ shoreward of the 100 m isobath. Although ice can cover the shelf year-round, more typically the inner shelf is ice-free from mid-July to mid-October. Based on archived National Weather Service records from Barrow and the climatology of Brower et al. (1988), westward (upwelling-favorable) winds predominate in all months, and especially from September through June. In July and August upwelling-favorable winds occur only slightly more frequently than downwelling winds. There has, however, been an appreciable increase in the frequency and duration of westward wind events over the ABS over the past two decades (Schulze and Pickart, 2012; Brugler et al., 2014). A few medium-sized (1–10 km^3 yr^{-1}) and numerous small arctic rivers enter the ABS along Alaska's North Slope. These drainages are entirely underlain by permafrost. Consequently, the annual river discharges, and especially the spring freshet, are brief due to rapid snowmelt and because the watersheds are completely frozen in winter, partially thawed for a brief period in summer, and do not support appreciable groundwater flow.

The purposes of this paper are to characterize and understand the processes that control the seasonal evolution of water properties and circulation over the inner shelf of the ABS with an emphasis on the landfast ice season. We also characterize the along- and cross-shore circulation and sea-level correlation scales and, where appropriate, compare these results with dynamical models of the LIZ under-ice circulation. The results should broaden our understanding of seasonality in this under-sampled portion of the Arctic Ocean and allow better insights on potential impacts on the LIZ associated with a warming Arctic. Our description is based on various data sets collected by different methods in different years as discussed in Section 2. In Section 3 we first provide an overview of the annual cycles of sea ice, currents, and water properties. We next examine several kinematic and dynamic aspects of the winter landfast ice season, explore aspects of the circulation at the landfast ice edge, and then describe features of under-ice freshwater plumes. Section 4 constitutes a discussion and summary of the results.

2. Methods

Our data derives mainly from seafloor-mounted oceanographic moorings *Dinkum*, *Reindeer*, and *Cross* deployed (Fig. 1b) in and offshore of Stefansson Sound in various years between 1999 and 2006. All moorings carried acoustic Doppler current profilers (ADCPs) and temperature/conductivity/pressure (T/C/P) recorders and some included transmissometers. Along-shore coverage was available in two years (2004–2006) from *Camden* deployed in Camden Bay (~120 km east of *Dinkum*) and in one year (2004–05) from *Smith* deployed in Smith Bay, ~235 km to the west of *Dinkum* (Fig. 1a). Deployment depths ranged from 7 to 17 m. *Dinkum* was the only mooring common to all years. The mooring positions, sensor packages, and bottom depths at each mooring used here are listed in Table 1. Sampling intervals were hourly or shorter. The moored data are supplemented with hydrographic measurements obtained during break-up in June 2001 and from late May to early June 2006, surface current measurements obtained during the open water season from a high-frequency radar (HFR) system in fall 2006, and from satellite-tracked drifters in August 2014. We also use the trajectories of several drifters deployed in the Chukchi Sea in fall 2012, which over-wintered in the LIZs of the ABS and Mackenzie shelf.

Moored instruments were mounted on compact frames constructed from fiberglass stock or Oceanscience Sea Spider stands. To limit the risk from ice keels, the top of the frames (ADCP transducers) were ~0.5–1.0 m above the seabed. Currents were measured with either a 1200 or 600 kHz Teledyne-RDI ADCP set in a gimbaled collar on the frame. The latter ensured that the ADCP remained vertical should the frame tilt from the horizontal by 20° or less (tilt sensors all indicated that the ADCPs remained level throughout their deployments except as noted). We used 0.5 or 0.25 m bin sizes on these upward-looking ADCPs. Ancillary instruments (Seabird, Inc. SBE16 SeaCats) and an acoustic release, which controlled a float and line used for recovery, were attached to the frames, each ballasted with 90 kg of lead. The design succeeded insofar as only 2 of 19 moorings deployed over the years were struck by ice (in one case with little damage to the instruments). One design problem is that the conductivity cells and acoustic release were within 20–30 cm of the seabed and thus affected by sediment re-suspension. The release mechanism was often impacted by sediments necessitating recovery by divers. Later deployments using vertically-oriented releases having the trigger mechanism held farther off the seafloor were more reliable. Bottom sediments, re-suspended by fall storms, infiltrated some of the conductivity cells rendering the salinity estimates unreliable over the remainder of the record. Finally, and in spite of the ballast, waves and currents associated with a severe storm in October 2006, inverted the *Dinkum* mooring and moved the *Cross* mooring about 200 m to the southwest of its original location. While the ADCP functioned well throughout the remainder of the *Cross* deployment, its conductivity cell was compromised by sediments.

Pre and post-calibrations of the T/C/P recorders were compared and incorporated in computing final values. Salinity was also compared with the freezing point from winter records. We estimate that the

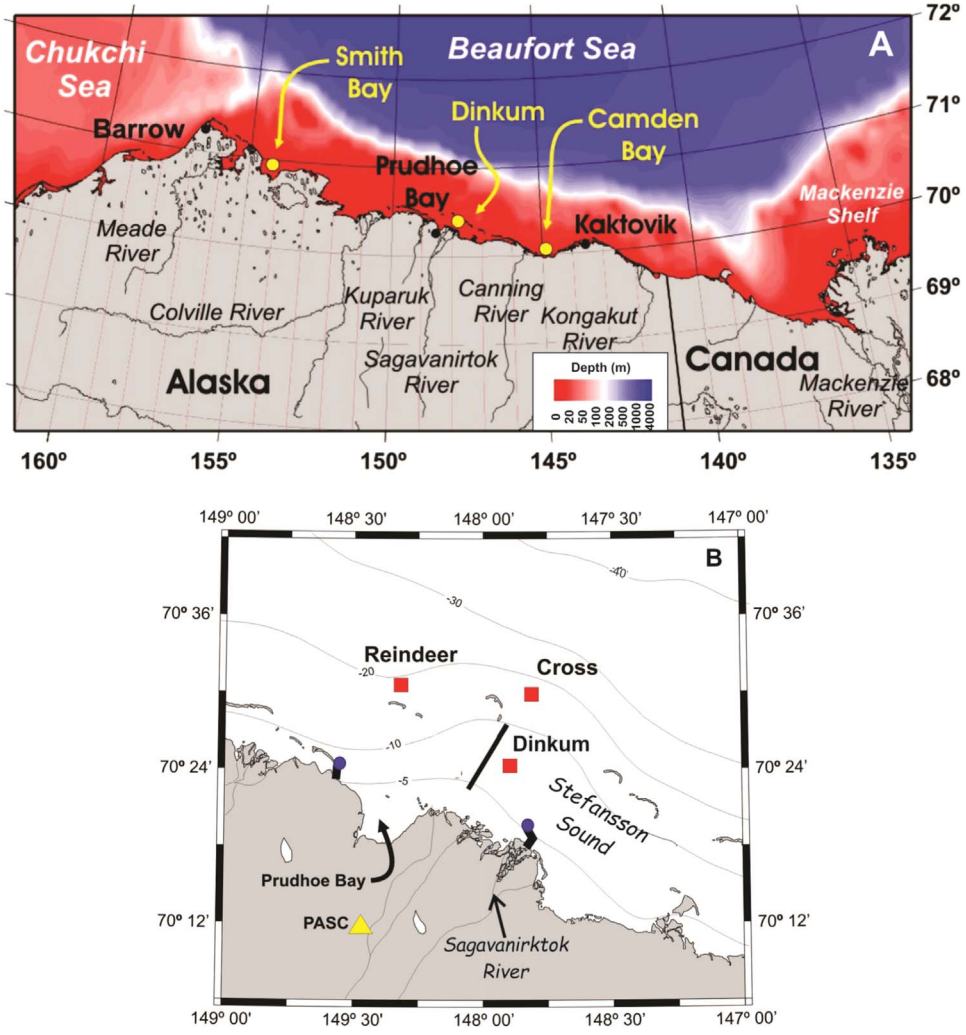

Fig. 1. A) Bathymetric map of the Alaskan Beaufort Sea (ABS) shelf showing location of geographic features and moorings *Smith*, *Dinkum*, and *Camden* (yellow circles), B) Inset map shows location of moorings *Dinkum*, *Reindeer*, and *Cross*, along with the location of the CTD section (black line) shown in Fig. 10 and the locations of the high-frequency radar sites (blue circles) in September - October 2006. PASC is the Deadhorse airport meteorological station. The NOAA tide gauge is co-located with the western radar site. (For interpretation of the references to color in this figure legend, the reader is referred to the web version of this article.)

salinity data is accurate to ~0.02 or better and temperature measurements are deemed better than 0.01 °C.

We estimated ice keel depth from the ADCPs based on the bottom depth, transducer height above bottom, and the range at which the intensity of the reflected acoustic signal was a maximum. We then multiplied the keel depth by the ratio of sea water density to sea ice density (1.12) to derive ice thickness. Noise in the ice thickness estimates due to discretization of the ADCP bins was reduced by smoothing the ice thickness estimates with a 5-day running mean.

CTD measurements using a Seabird SBE-25 were made through the

Table 1
Mooring and data sets used herein, including deployment period, locations, instrumentation (ADCP: 1200 and 600 kHz; SC = SeaCat), variables measured (**V** = velocity; T = temperature; S = salinity; P = pressure; Tr = transmissivity) and bottom depth.

Mooring name/Dates	Latitude (N)	Longitude (W)	Instruments	Variables measured	Bottom depth (m)
DINKUM					
8/99–9/00	70° 24.352′	147° 53.656′	1200 & SC	**V**, T, S, P, Tr	6.8
8/04–8/05	70° 24.437′	147° 53.656′	1200 & SC	**V**, T, S, P, Tr	6.8
8/05–9/06	70° 24.394′	147° 53.656′	1200 & SC	**V**, T, S, P, Tr	6.9
REINDEER					
9/01–8/02	70° 30.539′	148° 19.212′	1200 kHz	**V**	12.7
CAMDEN					
8/04–8/05	70° 1.692′	144° 56.584′	1200 SC	**V**, T, S, P	8.6
8/05–8/06	70° 1.707′	144° 56.617′	1200 SC	**V**, T, S, P	6.9
SMITH[a]	70° 59.288′	154° 1.994′	1200 SC	**V**, T, S, P	9.8
8/04–8/05					
CROSS[b]	70° 29.980′	147° 48.275′	600 SC	**V**, T, S[b]	17.3
9/06 – 8/08					
PASC	70° 11.7′	148° 27.7′	Anemometer	Winds	
NARR Grid Point	70°40′	148° 0.0	Model	Winds and Air Pressure	
NOAA Tide Gauge (Prudhoe Bay)	70° 24.7′	148° 31.9′	Water level	Sea level	

[a] Pressure erratic in late winter of 2005 and not used thereafter.
[b] CROSS was not recovered in 2007 due to inclement weather, but successfully recovered in August 2008.

ice in June 2000 along 7 stations extending northward from the mouth of the Sagavanirktok River (Fig. 1b) and in 2006, as break-up began, when near-daily CTD profiles were collected close to one of these stations. Based on pre- and post-calibration coefficients, the accuracy of the vertical profile salinity and temperature data are 0.01 and better than 0.01 °C, respectively.

We use two additional data sets to illustrate the rapidity by which waters on the inner ABS shelf can be exchanged during the open water season. The first was derived from a pair of 13 MHz high-frequency radar (HFR) systems deployed at two shore-based locations in the Prudhoe Bay area (Fig. 1b and described by Potter and Weingartner (2010)). This HFR pair had an effective range of ~50 km and a horizontal resolution of 2 km. The system's antennae patterns were calibrated per Barrick and Lipa (1986) and Kohut and Glenn (2003). The second data set consisted of 22 satellite-tracked Microstar drifters (manufactured by Pacific Gyre, San Diego CA) equipped with a CODE-type drogue (Davis, 1985) at 1-m depth. The drifters were deployed as a single cluster in a water depth of ~25 m about 10 km offshore of Kaktovik (Fig. 1a) in August 2014. Drifter positions, ascertained by GPS, and sea surface temperatures were measured hourly, recorded internally, and transmitted to shore via Iridium. Prior to analyses, we removed outliers in the position fixes and temperature and then interpolated the data to the top of each hour. The drifters released in the Chukchi Sea had drogues at 10-m depth, and their data were processed similarly.

Hourly wind data were obtained from the National Weather Service station at the Deadhorse airport (designated PASC and located at 70° 11.7′N, 148° 27.7′ W; Fig. 1b). In some years these were incomplete, so we used 3-hourly wind data from the North American Regional Reanalysis (NARR) models operated by the National Center for Environmental Prediction (NCEP; Mesinger and Coauthors, 2006) at a gridpoint near 70.4°N, 148°W. Additional sea-level data were obtained from the NOAA tide gauge in Prudhoe Bay (Table 1). Sagavanirktok River discharge measurements, collected by the United States Geological Survey, were made ~115 km upriver from the mouth.

We used Synthetic Aperture Radar (SAR) imagery from the November–December 2006 period to analyze the position of the landfast ice edge in conjunction with the *Cross* velocity record. We estimated this position subjectively from images separated by 2–3 day intervals by looking at feature displacements. Two analysts independently conducted the examination between successive pairs of images. The results from both analysts agreed in all cases.

3. Results

3.1. Overview of the annual cycle

We describe the annual cycle based on the *Dinkum* moored record from mid-August 1999 to late-August 2000. This record, which is representative of other moorings deployed within the LIZ, provides the best coincidental records of salinity and transmissivity amongst the various moorings. We first examine the time series of the ADCP-derived ice thickness, bottom-track velocity (surface and/or ice velocities), and the along-shore currents (Fig. 2) and then the water properties (Fig. 3). We differentiate between the landfast and open water seasons based on the ADCP bottom-track velocity (Fig. 2b). Large, noisy bottom-track velocities indicate open water and/or drifting ice floes. When landfast ice is present the bottom-track velocities are zero.

We begin by considering the time series of the ice thickness (Fig. 2a). In August 1999 the inner shelf was ice-free except for occasional drifting floes or sheets of melting ice as occurred for a few days at the end of the month. The ice disappeared by early September and the inner shelf remained ice-free until mid-October when ice began forming. Thickness increased steadily through fall and winter and attained its maximum value of ~2 m in early April. Ice thickness remained constant through late May, decreased rapidly in June, and effectively disappeared by the end of the month. The bottom-track velocities (Fig. 2b) indicate that the landfast ice season at *Dinkum* began on 15 October 1999 and ended on 30 June 2000, when ice began drifting. (Landfast ice formation commences at the coast and expands seaward, so the formation dates refer to the date when the ice extended offshore to the mooring location and not when it initially formed at the coast.)

The 5-year *Dinkum* record indicates that the earliest occurrence of landfast ice at this location was on 13 October 2001 and the latest was on 27 October 2004. The earliest and latest landfast breakout dates were 28 June 2005 and 5 July 2004, respectively. According to the bottom-track record, transitions between the two seasons occur abruptly. Time series of the unfiltered alongshore velocity component (directed along 119° and 299° for *Dinkum*; Fig. 2c) indicates that current speeds and current variance change with the transition from the open water to the landfast ice season. Current speeds are swift during the former period but weak during the latter. Histograms of current speed composited from all years and moorings (Weingartner et al., 2009) indicate that for the landfast ice season ~50% of the current speeds were ≤ 5 cm s^{-1} and only ~2% of the speeds exceeded 15 cm s^{-1}. Maximum under-ice current speeds were ~20 cm s^{-1}. In contrast, during the open water season, only 20% of the current speeds were ≤ 5 cm s^{-1} and more than 50% of the speeds exceeded 15 cm s^{-1}. Open water current speeds >50 cm s^{-1} occurred ~5% of the time and maximum current speeds were ~100 cm s^{-1}. During the landfast ice season the subtidal currents comprised 50–80% of the total variance, with the larger values typical of most records. By contrast, the subtidal variance accounted for more than ~85% of the variance during the open water season. In both seasons the subtidal circulation is alongshore polarized. The dominant tidal constituent (M_2) had a magnitude of ~2 cm s^{-1}; the magnitudes of other semi-diurnal and diurnal constituents were half this value.

The formation and ablation of sea ice and river runoff control the annual cycle of water property parameters (Fig. 3a, b). River discharge was small at the beginning of the record in August 1999 and diminished to negligible levels when rivers and the active layer re-froze by October and remained so through late May 2000. At that time the discharge increased, at first gradually into early June and then very suddenly over the next week when it attained its annual maximum of ~700 m^3 s^{-1}. Thereafter the discharge decayed gradually and reached ~150 m^3 s^{-1} by the end of June. The large discharge pulse surrounding the annual maximum constitutes the spring freshet, when >80% of the annual river discharge occurs. According to Rember and Trefry (2004) the freshet also carries more than 80% and 50% of the annual particulate and dissolved carbon and trace metal loads, respectively. Through the remainder of summer and fall, the runoff diminished, except for episodic discharge pulses following precipitation and/or snowmelt events.

It is clear from the discharge and ice thickness plots that these parameters coincide from late May through June. In part this covariance reflects the melting response to the seasonal increase in solar radiation and the increase in thawing degree-days. The landfast ice melt rate increases rapidly due to the large and sudden decrease in albedo at the ice surface as sediment-laden river waters overflow the ice adjacent to the coast (Dean et al., 1994; Searcy et al., 1996). The albedo change is critical in terminating the landfast ice season because it accelerates ice melt in the LIZ. Landfast ice begins drifting once stamukhi have melted.

Bottom temperatures (Fig. 3c) from August – September 1999 varied between 5 and 2 °C, but by late September decreased rapidly over a 10-day period to reach freezing (−1.7 °C) in early October, shortly before landfast ice was established. Freezing temperatures persisted from early October until late June 2000, whereupon temperatures increased to ~0 °C by late July after the ice disappeared. Bottom salinity (Fig. 3c) was variable and ranged from 20 to 31 throughout August – September. With the onset of freezing waters and ice formation, the salinity increased steadily and reached 34–35 by

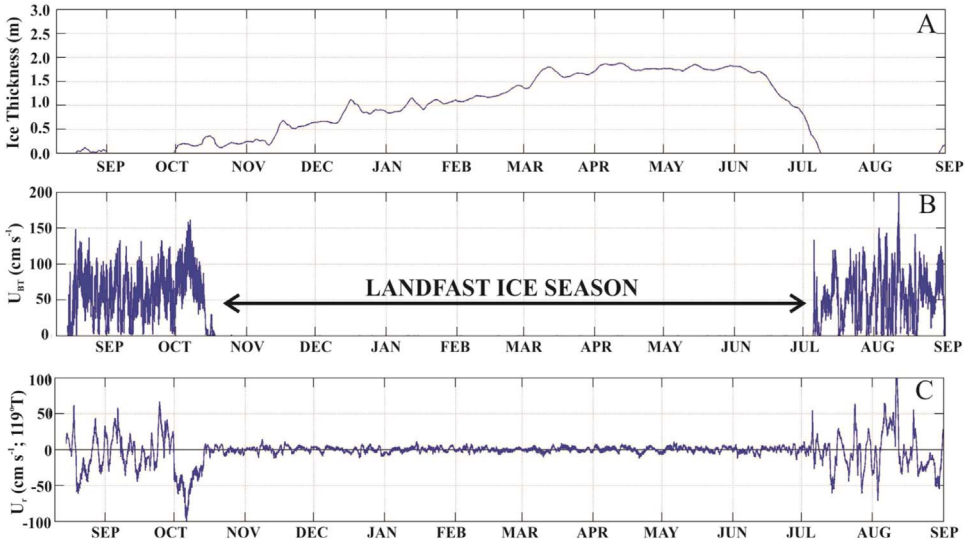

Fig. 2. The 1999–2000 *Dinkum* time series of A) ice thickness, B) bottom-track speed, and C) along-shore velocity.

January. Although ice continued to grow slowly, the salinity decreased to ~32.5 by mid-February, suggesting that even the weak under-ice currents can exert advective control on local LIZ property budgets. Salinity remained relatively constant from mid-February through mid-June and then, in conjunction with the disappearance of the ice, decreased rapidly to ~30 by the first week of July. By late July, solar heating, increased wind-mixing, and wind-forced currents combined to rapidly decrease bottom salinities to 20–24 and increase bottom temperatures to between 0 and 4 °C. These transitions herald the onset of the next annual cycle.

Transmissivity (Fig. 3d) also showed pronounced seasonality. Throughout late summer and fall it varied, due to wind events that re-suspended sediments via strong currents and/or waves. Transmissivity decreased to very low values coincident with the rapid formation of ice in early October. Again, these low values were associated with strong wind events that, in addition to forcing swift currents and large waves, also promoted cooling and frazil ice formation. In these shallow depths, frazil ice production during the initial stages of freeze-up causes sediment re-suspension (Reimnitz et al., 1990). Although some of this re-suspended material is carried away by the currents, a substantial fraction is incorporated into the forming ice (Barnes et al., 1982; Stierle and Eicken, 2002; Eicken et al., 2005b). Transmissivity is high throughout the landfast ice season, except in June when ice begins melting and discharge increases. After the ice disappears, transmissivity values increase again, until fall storms and cooling begin the process anew.

This overview of the annual cycle suggests that there are three distinct oceanographic seasons on the inner shelf of the ABS: the 8 month-long "winter" landfast ice season that extends from mid-October through May - June, a month-long melting season in June when landfast ice and runoff interact with one another, and the open water season that extends from mid-July through mid-October.

3.2. The winter landfast ice season

In this section we present kinematic and dynamic aspects of the winter landfast ice season and, where appropriate, make comparisons with the open water season. We begin by considering the time series of the NARR along-shore winds (which is generally within 15° of the zonal direction), the 35-h filtered and inverse barometer-corrected sea level

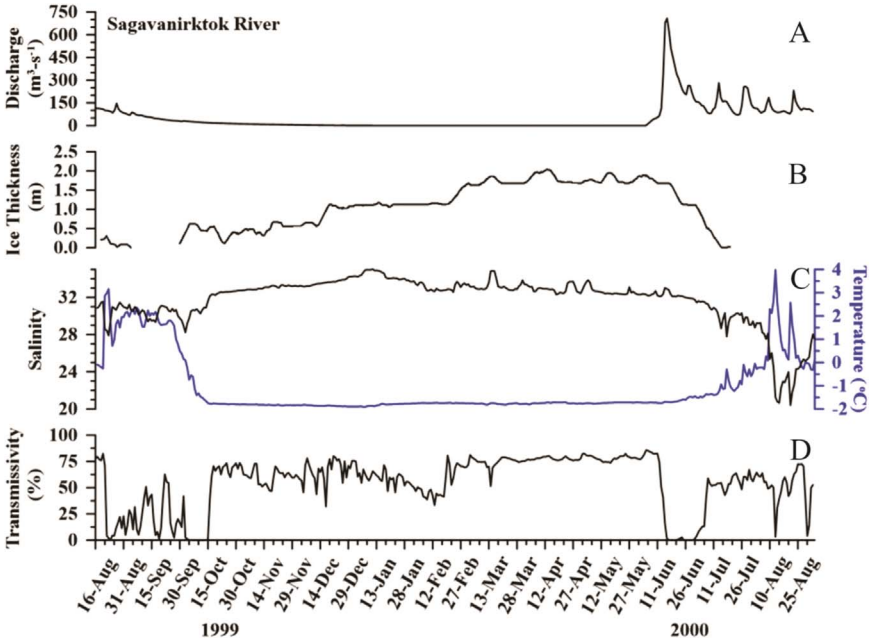

Fig. 3. The 1999–2000 time series of A) Sagavanirktok River discharge, B) *Dinkum* ice thickness, C) salinity and temperature, and D) transmissivity.

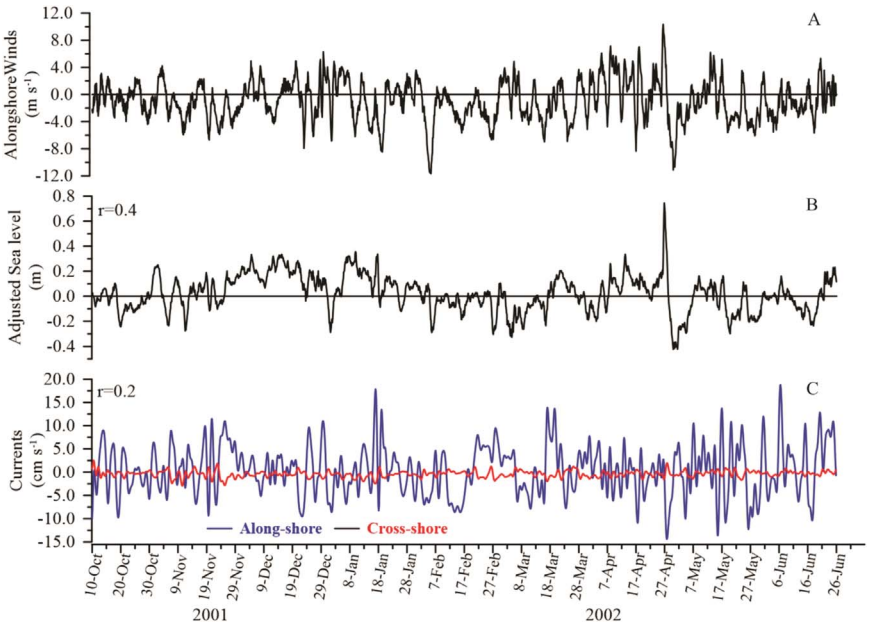

Fig. 4. 10 October 2001 to 27 June 2002 time series of A) the along-shore winds (NARR), B) the subtidal and inverse-barometer adjusted sea level (Prudhoe Bay), and C) the along-shore and cross-shore velocity components (in blue and red, respectively) at *Reindeer*. The correlation coefficients (r) between the along-shore winds and each variable are given on the left hand side of each plot. (For interpretation of the references to color in this figure legend, the reader is referred to the web version of this article.)

from Prudhoe Bay, and the 35-h low-pass filtered along- and cross-shore currents for the landfast ice period of 10 October 2001–26 June 2002 at Reindeer (Fig. 4). The along-shore winds account for ~90% of the wind variance, had typical speeds ≤ 5 m s^{-1}, and averaged ~1 m s^{-1} to the west. Sea-level anomalies (about the mean depth of 12.7 m) ranged between −0.4 and 0.6 m, but over most of the record they varied between ±0.2 m. Comparison of the wind and sea-level time series suggest some correspondence between the two, and for all sites, wind-sea-level correlations ranged from ~0.3 to 0.4 and were significant (i.e., $p < 0.05$) during the landfast ice season. For the open water season, the correlations between winds and sea level were greater (0.5–0.60; $p < 0.05$). Although there were large seasonal differences in current speeds, seasonal sea level variations were similar in magnitude. In both seasons, sea-levels fluctuated between ±0.5 m with root-mean-square values being ~0.2 m.

For most moorings and deployment periods (including *Reindeer*) the mean along- and cross-shore currents during the landfast ice season were ≤ 1 cm s^{-1} and, in all but a few cases, not significantly different from zero. Under-ice currents were quite variable, with integral time scales being ~2 days. At all moorings the correlation between along-shore winds and currents was not, or only weakly, significantly different from zero (for *Reindeer* the correlation was 0.2, $p < 0.05$). By contrast, open water season currents were significantly correlated with both winds and local sea level although the correlation coefficients varied across years and sites and ranged from ~0.5 to ~0.7.

There were also seasonal differences in the along-shore coherence scales as determined by the empirical orthogonal functions (EOFs) of the along-shore currents. The EOFs were computed separately for the landfast ice and open water seasons using the *Smith*, *Dinkum*, and *Camden* records from 2005 to 06. For the open water season the first mode explains ~90% of the variance, whereas during the landfast ice season this mode accounts for 50% of the variance.

Bottom pressure variations were coherent and in-phase during the landfast ice season for time scales >2 days and over the 119 km separating *Camden* and *Dinkum*. The along-shore velocity at *Dinkum* and the bottom pressure difference between *Dinkum* and *Camden* were also coherent and out-of-phase implying that along-shore pressure gradients and frictional stresses are important in the linearized and vertically-averaged along-shore momentum balance:

$$\frac{\partial U}{\partial t} - fV = -\frac{1}{\rho_0}\frac{\partial P}{\partial x} - \frac{(r_i + r_b)U}{H} \quad (1)$$

where U and V are the vertically-averaged along- and cross-shore velocity components, f the Coriolis parameter, t time, $\partial P/\partial x$ the pressure gradient in the along-shore direction (x), H the water depth, and ρ_0 a reference density. The stresses in the along-shore direction (τ^x) are parameterized by a linear stress law, $\tau^x = \rho_0(r_i + r_b)U$, with r_i and r_b being the resistance coefficients between the ice and the water and the seabed and the water, respectively. We assessed this relationship by neglecting the first term on the left, the local acceleration term, which is 1–2 orders of magnitude smaller than the pressure gradient. Our measurements did not extend across either boundary layer, which may contain cross-shore transports comparable, but opposite, to the interior cross-shore transport (Kasper and Weingartner, 2012). We thus neglect the vertically averaged Coriolis acceleration under the assumption that the boundary layer transports effectively cancel the interior transport. Moreover, bottom pressures (and gradients) were not coherent with V. Under these conditions, the force balance reduces to one between the pressure gradient and the stresses, i.e. $(H/\rho_0)\Delta P/\Delta x = -(r_i + r_b)U$, with $H = 5$ m and $\rho_0 = 1025$ kg m^{-3}. We assessed this balance by first low-pass filtering bottom pressures and alongshore velocity to eliminate fluctuations at periods ≤2.5 days. Filtering reduced the sub-inertial velocity variance by 50% (2004-05) and ~35% (2005-06).

We examined the relationship using U at *Dinkum* and the bottom pressure difference between *Camden* and *Dinkum* for the time period between 1 November and 31 May of each year shortly after landfast ice formed at each site and before break-up and significant runoff began. Fig. 5 shows the results for three separate time periods along with the linear fits. There are two points of note. First, there was no significant relationship ($p < 0.05$) for the period between 1 Nov 2004 and 13 Jan. 13 2005 (and data for this period are not plotted). Second, there is an offset in the two regressions for the winter of 2005. These caveats may be due to a spatially-variable width and/or ice breakout events in the LIZ between *Dinkum* and *Camden* over these portions of the record, which would result in pressure gradients over shorter scales. Nevertheless, the fits were all significant ($p < 0.05$) with r^2 ranging from 0.40 (2005-06) to ≥0.80 (2005). The slopes, the sum of the two resistance coefficients, range from 5.8 to 7.6 × 10^{-5} m s^{-1}. Both slopes from the winter of 2005 were statistically identical. The 2005-06 data were more variable with a weaker fit (although its confidence interval overlaps with the one for the first period in 2005).

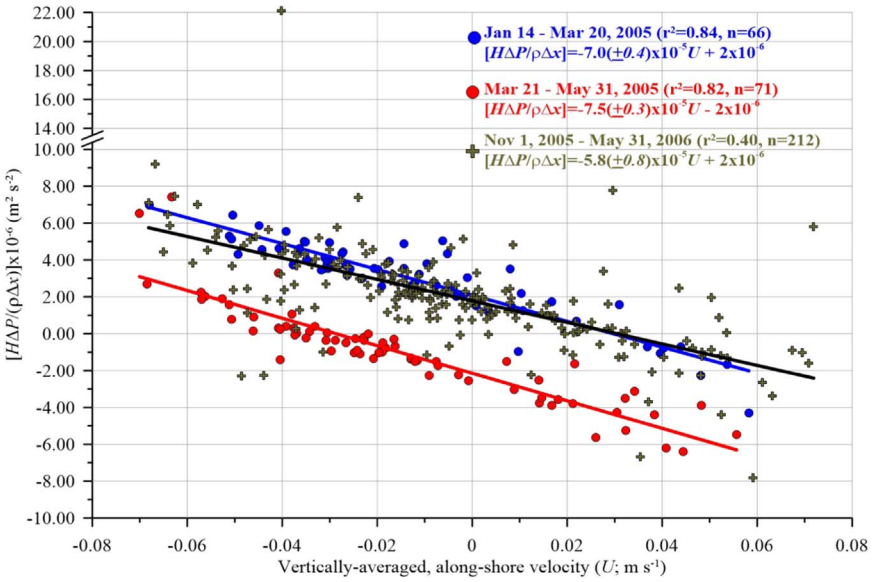

Fig. 5. Vertically-averaged along-shore momentum balance accompanied by linear regression results for each period.

3.3. Vertical current structure

We examined the vertical structure of the along-shore flow during the landfast ice season by compositing profiles segregated by the along-shore flow direction defined by the principal axis orientation (nominally eastward and westward). In general these are Poiseuille-like with maximum speed centered approximately midway between the seabed and the underside of the ice. The velocity profiles were weakly sheared (at least outside of the under-ice and bottom boundary layers, neither of which were resolved by our measurements) with velocities generally varying by ~1 cm s^{-1} over the depth of the water column. The archetypal parabolic velocity profile is shown in Fig. 6a, which was constructed by averaging all westward (toward 293 °T) flow events for February 2007 from *Cross*. By contrast, the mean eastward (toward 113°T) velocity profile is quite different (Fig. 6b). It increased linearly from 1 cm s^{-1} at ~2 m below the ice to ~6 cm s^{-1} at 14 m depth. The directional differences in the profiles suggest that a substantial ice keel was east of *Cross,* which blocked flow in the upper water column and intensified the near bottom flow. *Cross* was deployed on the ~17 m isobath and was the farthest offshore mooring in our study. As such, its complicated velocity profile may be typical of the distal regions of the LIZ where ridging and stamukhi tend to be concentrated.

3.4. Circulation at the landfast ice edge

The *Cross* record also afforded an intriguing glimpse of the cross-shore circulation variability associated with the landfast ice edge. We show this using a subset of 2006 Synthetic Aperture Radar (SAR) images collected between 11 November and 22 December (Fig. 7a–f). Each image shows the location of mooring *Cross* (yellow dot) in relation to the landfast ice-edge location indicated by the red line. The SAR images allowed us to estimate the distance between the mooring and the ice edge, which facilitate interpretation of the time series of along-shore winds and currents and the bottom-track record for the 1 September - 31 December 2006 period (Fig. 8).

From 1 to 15 September a broad band of melting ice covered *Cross*. This ice sheet had grounded along the seaward side of several of the barrier islands bordering Stefansson Sound and was evident in the bottom-track records, in visible satellite imagery, and by local observers. By 15 September the ice sheet largely dispersed and open water

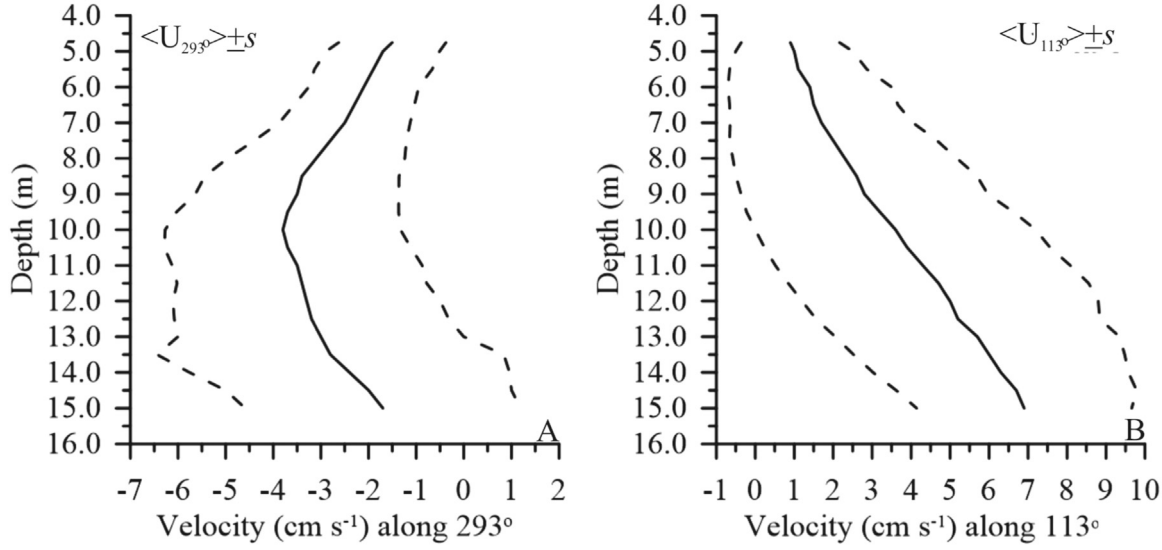

Fig. 6. Mean along-shore velocity depth profiles for *Cross* for February 2006. The plots depict the mean profile constructed from all westward (A) and eastward (B) flow events. Dashed lines bracket one standard deviation about the mean.

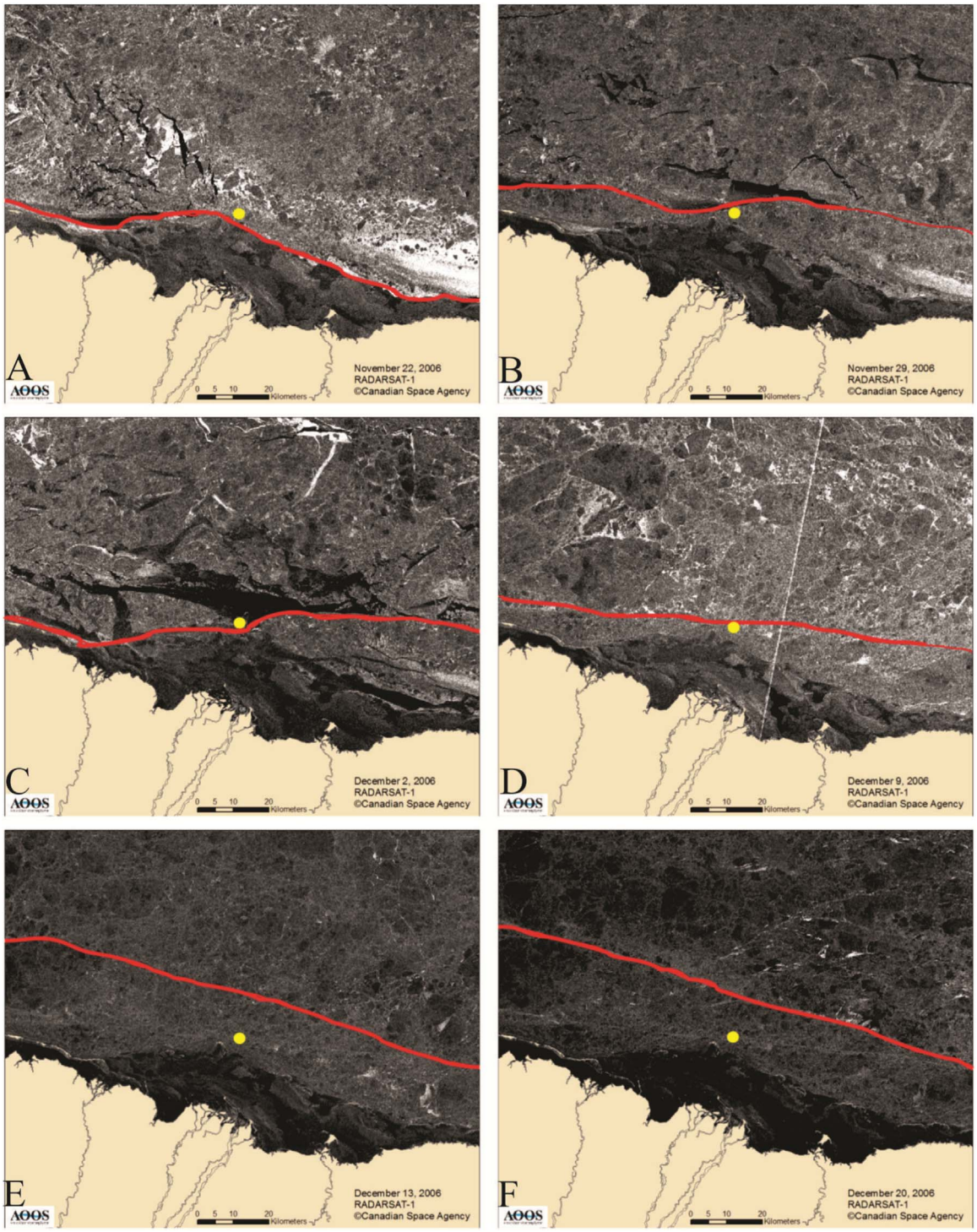

Fig. 7. SAR imagery from A) 22 Nov., B) 29 Nov., C) 2 Dec., D) 9 Dec., E) 13 Dec., and F) 20 Dec., 2006 of the estimated location of the landfast ice edge (red line) with respect to mooring *Cross* (yellow dot). (For interpretation of the references to color in this figure legend, the reader is referred to the web version of this article.)

and/or drifting ice enveloped *Cross*. These conditions persisted until landfast ice, which had been expanding seaward from the coast beginning in late October, covered *Cross. Cross* was briefly covered for ~2 days on ~17 November and then more frequently after 23 November. From mid-September through mid-November, the along-shore currents were swift and positively correlated with the along-shore winds consistent with our depiction of the open water season circulation. Landfast ice covered *Cross* from 23 November through 1 December, during which time the currents were eastward and weak at ~5 cm s^{-1}, while the winds were westward at 7–10 m s^{-1}. Note that the SAR images throughout this period suggest that the mooring was within 1–4 km of the ice-edge. From 2 to 10 December the landfast ice retreated shoreward exposing *Cross* to drifting ice while the winds varied from eastward to westward at 5–10 m s^{-1}. Current velocities were again coherent and in-phase with the winds, and current speeds were substantial (~35 cm s^{-1}) and much greater than those measured several days earlier beneath the landfast ice. Beginning 11 December the landfast ice expanded rapidly offshore with the ice edge ~12 km seaward of *Cross* by 13 December. The ice-edge remained at this location through at least 22 December during which time the currents were

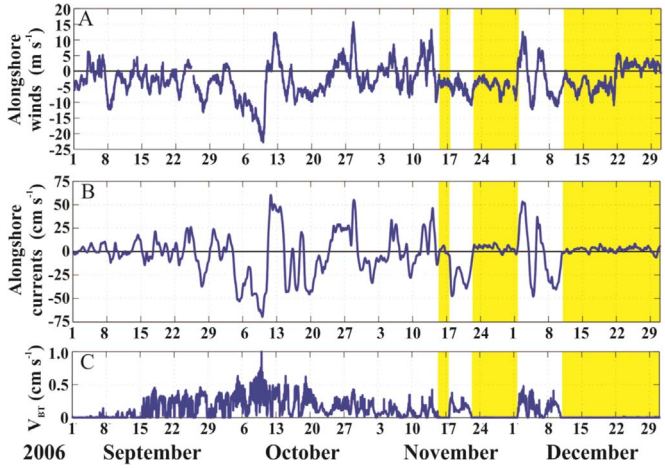

Fig. 8. Time series of A) along-shelf winds (positive eastward), B) along-shelf currents (positive eastward), and C) ADCP bottom track return from *Cross* for the period 1 September - 31 December 2006. The regions shaded yellow indicate when landfast ice (LI) covers the mooring after 16 November. (For interpretation of the references to color in this figure legend, the reader is referred to the web version of this article.)

weakly eastward and winds were westward and often quite strong. Hence from 23 November to 1 December and from 12 to 22 December, landfast ice covered the mooring, and the currents were weak and anti-correlated with the winds, in agreement with the model results of Ohshima (2000) and Kasper and Weingartner (2012) for regions well within the LIZ. After 22 December, however, the winds remained westward, but the currents within the LIZ reversed and flowed down-wind, in contrast to both models' predictions. Throughout the remainder of the landfast ice season there was no statistically significant relationship ($p < 0.05$) between currents and winds similar to the results obtained from other moorings during the landfast ice season.

The preceding discussion implies that there is a strong cross-shelf horizontal velocity gradient that straddles the ice-edge as predicted (Ohshima, 2000; Kasper and Weingartner, 2012). The current record and SAR imagery allow estimating the ice-edge Rossby number, Ro, $\partial u/f\partial y \Rightarrow \Delta U/fL_y$. Here, L_y is a characteristic cross-shore length scale over which the along-shore velocity changes by ΔU. Along-shore current shears of ~50 cm s^{-1} over a cross-shore distance of 1 − 2 km, as suggested by the SAR images, yields an $Ro \sim 0.4$. These values of L_y, which are considerably smaller than the 7–15 km barotropic radii of deformation for water depths of 10–20 m, are probably not unusual throughout the winter, especially when winds are strong, and the transition zone between landfast ice and the drifting pack is narrow. Consequently landfast ice-edge jets are non-linear, and potentially barotropically unstable.

3.5. The break-up season

The break-up season occurs when the landfast ice and spring runoff interact with one another, and represents the transitional period between the winter and open water seasons. Our break-up description is based on the May–June 2000 time series of the ice thickness, transmissivity, velocity, and vertical shear in the horizontal velocity from *Dinkum* in conjunction with the Sagavanirktok River discharge for the same period (Fig. 9a). As noted, the spring freshet occurred for 12 days; it began on 7 June, peaked 3 days later, and decayed to pre-peak levels by 18 June. Each of the other time series in Fig. 9 show abrupt changes coincident with the freshet. For example, the ice thickness (Fig. 9b) was ~1.8 m from the beginning of May through 10 June but then decreased, at first gradually and then more rapidly towards the latter half of the month. Similarly, transmissivity (Fig. 9b) values fell from ~75% on 12 June to 0% on 16 June and were negligible throughout the rest of the month. These low values cannot be explained by sediment resuspension by currents because currents remained weak. Rather the high turbidity was probably due to sediments released from the melting ice or settling out of under-ice river plumes. Cross- and along-shore velocity shears (Fig. 9c) were small (< 0.01 s^{-1}) throughout May, but these increased nearly fourfold in conjunction with the spring freshet. The increase in the cross-shore velocity shear was associated with a large increase in offshore velocity at ~2 m depth (Fig. 9d). Recall that cross-shore current speeds are typically ~1 cm s^{-1} during the landfast ice season, but these increased to 5–10 cm s^{-1} between 10 and 15 June and were the largest observed during the landfast ice period.

The June 2001 CTD section provides another perspective on water column processes during the landfast break-up season. River discharge and landfast ice melt promotes stratification, and indeed the sub-ice water column was strongly stratified (Fig. 10a) by a 1-m thick pycnocline centered ~2.5 m below the ice. In the upper 2 m temperatures and salinities were −0.2 °C and 3–5, respectively, while below the pycnocline the respective values were < −1.6 °C and > 32. Transmissivity was very low (< 10%) in the upper 2 m and increased rapidly across the pycnocline to > 70% below 3 m. Fig. 10b shows time series of the vertical profiles of temperature and salinity between 22 May and 3 June 2006 taken close to the station marked with an arrow in Fig. 10a–c. These data were collected before overflow flooded the ice surface and drastically changed the albedo. River discharge was negligible on 22 May, and the water column was vertically uniform with respect to temperature (< −1.7 °C) and salinity (32.5–33). Bottom water properties remained nearly constant throughout the sampling period. Discharge increased to 40 m^3 s^{-1} on 24 May, by which time the water column had developed a 2-layer structure. In the surface layer salinities were ~11 and temperatures were −0.6 °C. Thereafter, discharge rapidly increased to a maximum of 400 m^3 s^{-1} on 3 June. Over the 9-day period from 24 May to 3 June, salinities within the well-mixed portion of the plume decreased to ~3 or less, and temperatures varied from −0.2 to 0.2 °C. The plume also thickened from 2 to 3 m depth by 3 June, which implies an entrainment rate of 10^{-6} m s^{-1}.

After plume formation, plume temperatures averaged ~0.1 °C above the freezing point. We assessed the role of the plume on under-ice melting by calculating the heat flux from the ocean to the ice following McPhee et al. (1999):

$$F_{oi} = \rho_o c_p (\widehat{V_0}/\widehat{\Gamma}) c_H \Delta T \tag{2}$$

where F_{oi} is the heat flux from the ocean to the ice, ρ_o is the plume density (1010 kg m^{-3}), c_p is the heat capacity of seawater (3990 J kg^{-1} °C^{-1}), c_H is the heat exchange coefficient (5.6×10^{-3}), ΔT is the difference between the freezing point temperature and the plume temperature, and $\widehat{V_0}$ is the water velocity vector (in complex form) outside of the under-ice boundary layer (0.05 m s^{-1}; cf. Fig. 9). The variable $\widehat{\Gamma} = \widehat{V_0}/\widehat{u_{*0}}$, where $\widehat{u_{*0}}$ is the (complex) friction velocity. The latter depends upon the under-ice roughness length, z_0 for which we have no information. Shaw et al. (2008) report values of u_{*0} ranging from 10^{-2} to 10^{-3} m s^{-1} based on measurements from the central Arctic basin. We evaluated Eq. (2) for $|\widehat{\Gamma}| = 5$ and $|\widehat{\Gamma}| = 50$ yielding heat fluxes between 2 and 22 W m^{-2}. The higher value implies a melt rate of 6 mm/day and is probably an upper bound given that we expect very smooth ice (small u_{*0}) close to the coast. By comparison, the net radiation at the top of the ice in late May and early June is ~100 W m^{-2}, yielding a melt rate of ~3 cm/day. Assuming that the meltwater at the ice surface drains into the plume, we estimate the depth-averaged salt balance for the plume over the 11-day period of 24 May–3 June:

$$\underbrace{\frac{\Delta S_p}{\Delta t}}_{a} = \underbrace{-v\frac{\Delta S}{\Delta y}}_{b} + \underbrace{\left[w_e(S_a - S_r) + \frac{\Delta h_i}{\Delta t}(S_i - S_r)\right]/h_p}_{c \quad d} \tag{3}$$

Term a is the rate of change of plume salinity ($\Delta S_p = 8$); term b describes the cross-shore advection of salt; and terms c and d are salinity changes due to entrainment and ice melt, respectively. The variables S_r, S_a, and S_i are the salinities of the river inflow (0), ambient

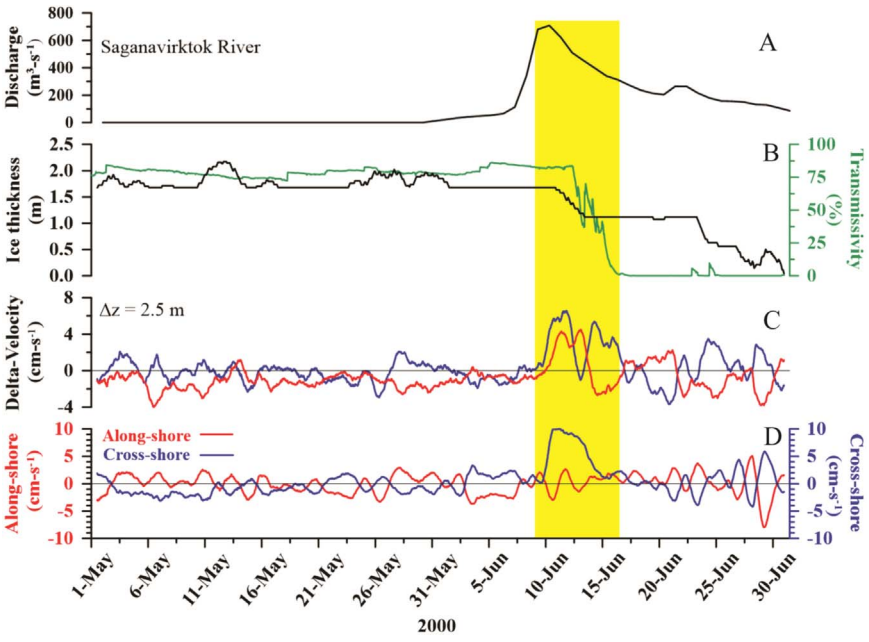

Fig. 9. May–June 2000 time series from *Dinkum* of A) Sagavanirktok River discharge, B) ice thickness (black) and transmissivity (green), C) along- and cross-shore vertical velocity differences, and D) along- and cross-shore velocities. The along- and cross-shore velocities are blue and red, respectively in C and D. (For interpretation of the references to color in this figure legend, the reader is referred to the web version of this article.)

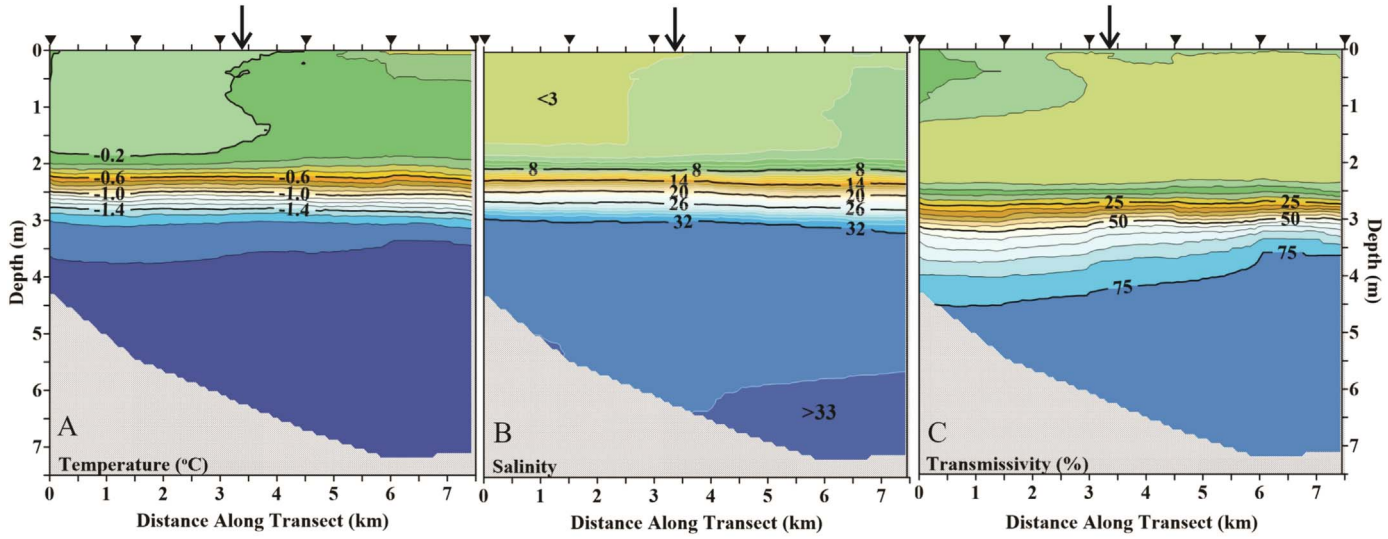

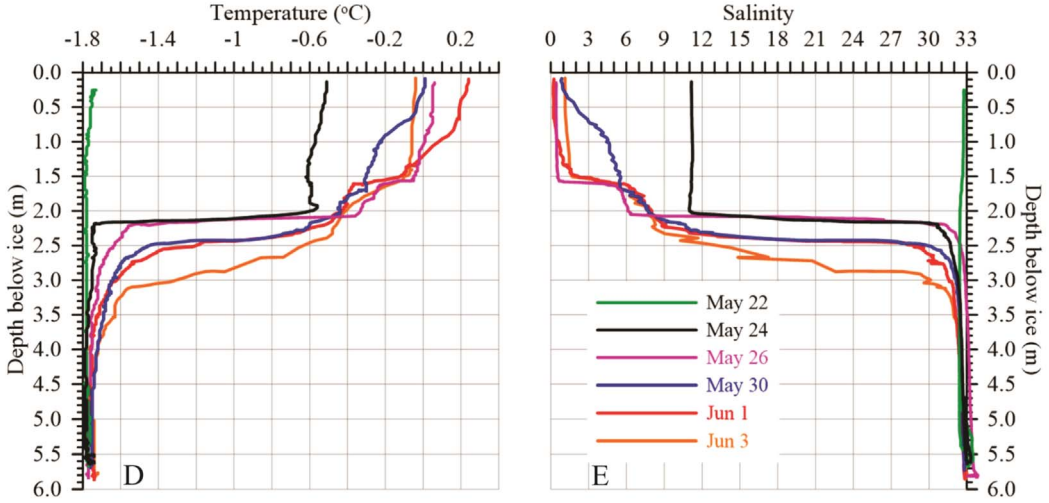

Fig. 10. The 6 June 2001 vertical section of: A) temperature, B) salinity, and C) transmissivity. The section extends from inshore (left) to offshore (right) and its location is given in Fig. 1b. Inverted triangles at the top of each panel indicate the location of the each of the 6 CTD casts that comprised the section. Panels D and E are time series of vertical profiles of temperature and salinity, respectively for the indicated dates in 2006. This station was located near the third inshore station shown by the vertically-oriented arrow in the top row.

water (32.5), and first-year ice (7). The entrainment rate is w_e; $\Delta h_i/\Delta t$ is the ice melt rate; y (v) is the cross-shore co-ordinate (velocity); and h_p is the plume depth (2.5 m). The observations suggest a salinity decrease of 0.9 day^{-1} over the 11 days. Plume salinity increased at ~1.1 day^{-1} through entrainment and ~0.1 day^{-1} from ice melt. The imbalance is satisfied if cross-shore advection freshens the plume at a rate of −2.1 day^{-1}. For a plume velocity of 5 cm s^{-1} the cross-shore salinity gradient would be ~5 × 10^{-4} m^{-1}, or ~5 per 10 km. This estimate seems reasonable based on the cross-shore salinity gradients reported by Alkire and Trefry (2006) and Trefry et al. (2009).

Our CTD measurements captured only a small portion of the under-ice plume. The measurements of Alkire and Trefry (2006) indicate that a similar plume, derived from the Kuparuk and Sagavanirktok rivers, extended ~17 km offshore. In their model study, Kasper and Weingartner (2015) modeled under-ice plumes fed by an idealized spring freshet. They found that the plume mixes very slowly due to ice-ocean friction and that the plume remains intact until crossing the landfast ice edge. Based on the shears and stratification (Figs. 9 and 10a and b), the bulk Richardson number was >300. Given the absence of wind mixing, and that vertical shears and tidal currents are weak, the quiescent conditions of under-ice plumes presumably allow much of the suspended material to settle quickly.

Under open water conditions, the energy required to homogenize the 2-layer structure of Fig. 10 to a depth of 6 m is ~540 J m^{-2}. Denman and Miyake's (1973) formulation for wind mixing suggests that it would take ~35 days to completely mix the plume to 6 m given typical July and August wind speeds of 5 m s^{-1}. If the Ekman transport is largely confined to this depth, then the plume, if subjected to an upwelling favorable wind event of 5 m-s^{-1} for 4–5 days, would be displaced 30–40 km offshore (~half the shelf width) over this period. Hence, the plume should remain largely intact during its offshore displacement.

4. Discussion

Our results suggest that the inner shelf of the ABS experiences three dynamically distinct seasons: “winter”, “break-up”, and “open-water”. The winter season begins with ice formation in fall (~mid-October) and ends in spring (late May/early June) with the onset of the spring freshet. The month-long break-up season concludes when the landfast ice detaches from the bottom and begins drifting. Break-up is followed by the ~3-month long open water/drifting ice season and ends when landfast ice forms again. Arguably, the open-water season could be further sub-divided, with both wind and buoyancy important from July to August and wind dominating in September and October.

The numerous biogeochemical transformations on Arctic shelves discussed by Macdonald and Yu (2005) are affected by advective exchanges. Our results imply that the ABS LIZ waters undergo little along- and cross-shelf exchange in winter in agreement with LIZ circulation models (Ohshima, 2000; Kasper and Weingartner, 2012) that assume ice sheets of uniform thickness and width. Exchange is further restricted by stamukhi, or deep keels at the LIZ ice edge (Macdonald and Carmack, 1991; Macdonald et al., 1995) and by ice edge fronts associated with horizontal current shears or those that might develop in conjunction with freezing in flaw leads (Melling, 1993; Macdonald et al., 1995; Dmitrenko et al., 2005).

A consequence of limited exchange is that winter LIZ water properties may depend on conditions established by horizontal advection at the time of landfast ice formation. These advective events can be substantial as illustrated by two examples. Fig. 11a shows the mean surface circulation, determined by HFR, over the inner shelf for 28 September - 22 October 2006 along with time series of the along-shore winds and surface currents at a single point within the radar mask (Fig. 11b). Over most of this period winds were >10 m s^{-1} and varied between easterly and westerly with surface currents tracking the winds. The mean winds and currents for this time period were westward at 10 m s^{-1} and 20 cm s^{-1}, respectively. If the surface current speeds are representative of those over the water column then the 25-day mean along-shore transport within the radar mask was ~0.2 Sv westward, enough to replace more than half the volume of the ABS shelf inshore of the 40 m isobath. A second example is illustrated by the mean trajectory of 22 drifters released on 8 August 2014 near Kaktovik (Fig. 12). The drifters moved ~375 km northwestward across the mouth of Barrow Canyon in 20 days in response to sustained northeasterly winds of ~10 m s^{-1} and possibly also to local dynamics operating at the canyon mouth. This drift included a substantial offshore component, which would carry fresh inner shelf waters into the Arctic Basin, consistent with the findings of Guay and Falkner (1998) and Macdonald et al. (1999). Both examples suggest that, in fall, the Mackenzie shelf is a substantial source of the water that forms landfast ice on the ABS.

There are other possible source waters and ice for the Beaufort LIZ. Volkov et al. (2002) and Mahoney et al. (2007a) showed that another mechanism for the offshore expansion of the LIZ is due to pack ice incorporation along its seaward boundary. The waters forming this ice may derive from a variety of sources, including the basin and the Chukchi shelf. An example of the latter is given by the trajectories of three 10-m drogued drifters that were deployed on the Chukchi shelf in August 2012 (Fig. 13). All three drifters moved eastward from the Chukchi and through Barrow Canyon by early September and then eastward along the shelfbreak. In early November, each drifter was trapped by drifting ice and moved back onto the Beaufort shelf where each was incorporated into the LIZ and remained immobile through winter. Drifters 6 and 11 overwintered on the ABS while drifter 5 was entrapped by in the Mackenzie LIZ.

Our results suggest that sediment transport processes on the ABS appear closely tied to the freeze and thaw cycle and consist of four temporally discontinuous processes. First, terrestrial material released with the spring freshet settle in the LIZ. Second, sediments are re-suspended and transported by currents and waves during the open water season, especially during fall storms (cf. Figs. 11 and 12). Hence, there is a 3-month time lag between the sediment accumulation in spring and fall re-suspension. The third step occurs during freeze-up, when sediments adhering to frazil ice are incorporated into the forming landfast ice. We expect little sediment transport for the next 8 months when currents are weak. The final step begins with spring break-up when sediment-laden ice either melts in-situ and releases its sediment load or is advected out of the region. The latter fate is suggested by the summer trajectories of drifters 5, 6, and 11 (those of Fig. 13), which overwintered in the LIZ. Fig. 14 shows three regional Moderate Resolution Imaging Spectroradiometer (MODIS) images from May through July 2013, on which are superimposed the trajectories of the ice-embedded drifters along with our estimate of the offshore location of the LIZ. The 20 June image indicates that Drifter 6 was in ice that apparently broke free of the LIZ earlier in the month although the drifter barely moved after detachment. Drifters 6 and 11 began moving westward by 26 June, while drifter 5 remained within the Mackenzie LIZ. By early July, however, all drifters were moving westward with the ice. They eventually melted free of the ice, Drifter 5 by mid-July on the ABS and Drifters 6 and 11 in late July on the Chukchi shelf.

We found strikingly large seasonal differences in the spatial correlation structure of the currents and their relationship to winds and sea level. Winds, sea level, and along-shore currents were significantly correlated with one another during the open water season but only weakly so (at best) during the LIZ season. To lowest order the under-ice momentum balance is between along-shore pressure gradients and frictional stresses. Our derived bottom and friction coefficients, which sum to ~7 × 10^{-5} m s^{-1}, are smaller than those used by Kasper and Weingartner (2012). Our estimate was based on measurements near-shore where the landfast ice is smooth. Similar measurements, made under rougher ice farther offshore, may yield larger values.

The reasons for these seasonal correlation differences are not entirely clear. Weak under-ice currents may account for some of the

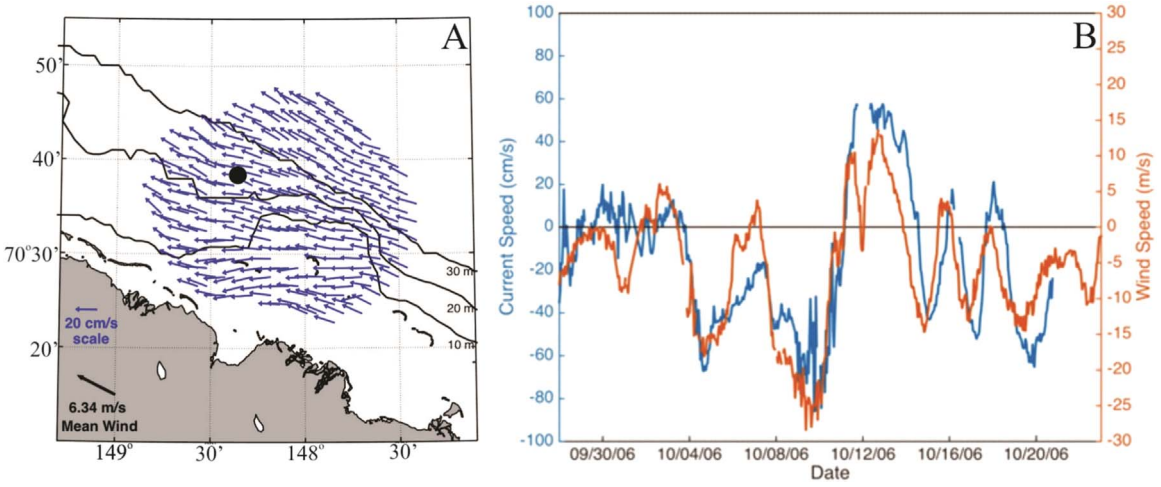

Fig. 11. A) HFR-derived map of the 28 September - 22 October 2006 mean surface currents and B) time series of the along-shore component of the winds (red) and currents (blue) at the HFR gridpoint indicated by the solid circle on the map to the left. (For interpretation of the references to color in this figure legend, the reader is referred to the web version of this article.)

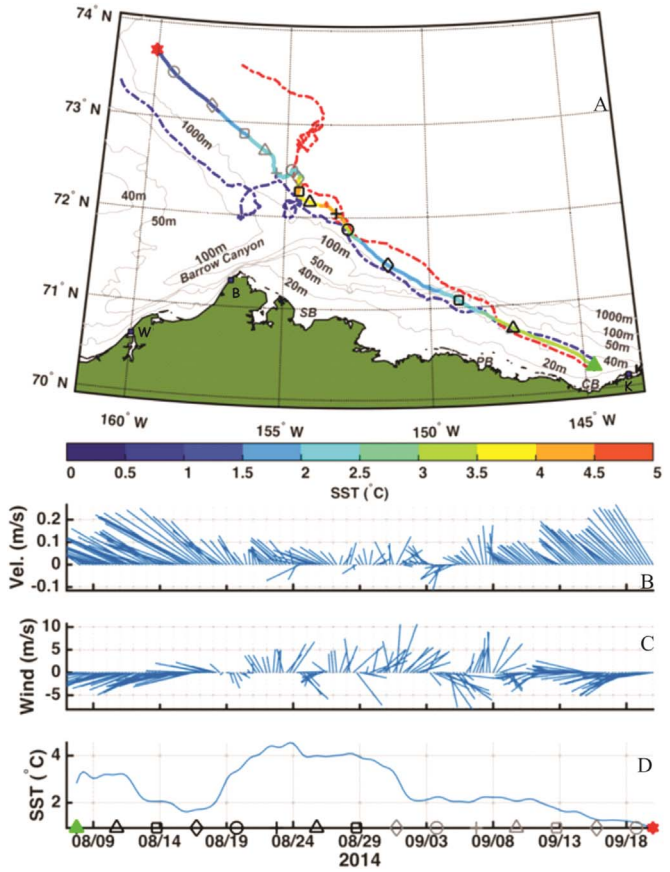

Fig. 12. A) Bathymetric map of the northeast Chukchi Sea and ABS with the mean trajectory of 22 satellite-tracked drifters (drogued at 1-m depth) and time series of the B) current, C) wind vectors and, D) sea surface temperature (SST). Drifters were released on 6 August 2014 offshore of Kaktovik at the location denoted by the green triangle and moved westward beyond the red star indicated on the figure. The mean trajectory is color-coded according to the SST and the symbols along the trajectory are at 3-day intervals corresponding to the dates on the *x*-axis of the SST plot. The dashed trajectories are of two drifters in the cluster to provide a sense of cluster dispersion with time. Place names are the villages of Wainwright (W), Barrow (B) and Kaktovik (K) and Smith (SB), Prudhoe (PB), and Camden (CB) bays. (For interpretation of the references to color in this figure legend, the reader is referred to the web version of this article.)

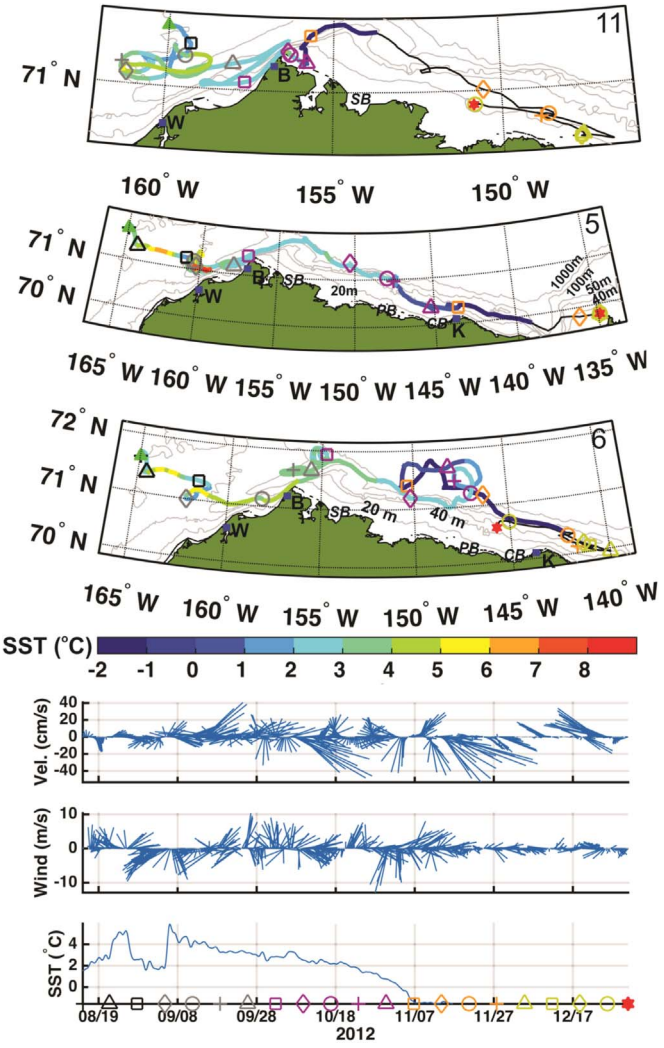

Fig. 13. Map showing the trajectory of satellite-tracked drifters (drogued at 10-m depth) 11, 5, and 6 that were released in August 2012 in the Chukchi Sea and became entrapped in the landfast ice of the ABS and/or Mackenzie shelf. The time series are those for drifter 6 and the symbols along each track correspond to the dates on the SST *x*-axis. Drifters were deemed in ice when the temperature records were < -1.8 °C.

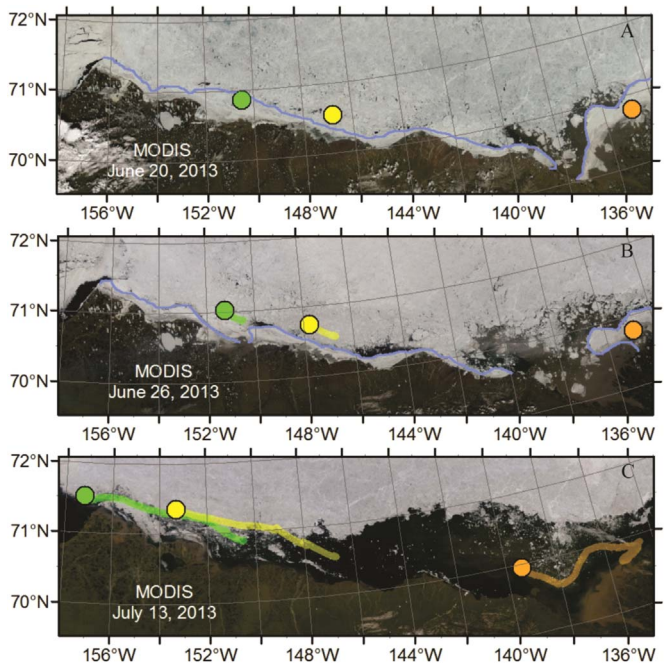

Fig. 14. A sequence Moderate Resolution Imaging Spectroradiometer (MODIS) images from 2013 during break-up of the LIZ. The positions and trajectories of drifters are superposed for A) 20 June, B) 26 June, and C) 13 July. These drifters are the same as those in Fig. 13 that overwintered in the LIZ and are orange (5), yellow (6), and green (11). The blue line in each panel denotes the approximate boundary of the landfast ice edge on the date indicated. (For interpretation of the references to color in this figure legend, the reader is referred to the web version of this article.)

degradation, but this explanation cannot apply to the change in wind and sea level correlation because sea level fluctuations during the landfast ice season were similar in magnitude to those of the open water season. Kasper and Weingartner (2012) suggested that such differences could arise due to along-shore variations in the LIZ width and to under-ice topography, which can vary over horizontal scales ranging from a few meters to tens of kilometers (Mahoney et al., 2007b).

Spatial variations in LIZ width (as suggested by the SAR [Fig. 7] and MODIS [Fig. 14]) images and roughness will result in patchy surface stresses. This patchiness would lead to a corrugated along-shore pressure field and circulation convergences/divergences on length scales smaller than the spatial scales of variability of the wind. Our moorings appear to have been too far apart to resolve adequately the along-shore velocity and pressure gradient scales in winter.

Circulation models are now beginning to address the complex ice dynamics of LIZ basal stresses (Lemieux et al., 2015), which along with air temperature, the thickness of the snow cover on ice, and winds (Divine et al., 2004) affect deformation (Tucker et al., 1979) and migrations of the LIZ ice-edge (Mahoney et al., 2007a). In addition, LIZ retreats and/or break-out events may also involve ice-edge deformations induced by the sheared ice-edge jets described here and by Dmitrenko et al. (2005) and Mahoney et al. (2007b).

5. Conclusion

The annual freeze-thaw cycle that governs runoff and the formation and ablation of landfast ice controls the seasonality in circulation and water mass properties in the nearshore Alaskan Beaufort Sea. In winter, the water column is at the freezing point, under-ice currents are weak, and cross-shore exchange appears minimal. Current variations are a response to along-shore pressure gradients, which appear to vary over length scales of $<\sim$100 km and over time scales of days. We hypothesize that the spatial scales of variability are associated with the changes in LIZ width and under-ice topography, both of which affect the response to time-varying remote and local winds. Horizontal current shears are very large along the seaward boundary of the LIZ and may support barotropic instabilities and the structure of the landfast ice edge. During the break-up season, river influxes stratify the inner shelf and under-ice plumes spread offshore in response to frictional coupling with the underside of the ice. The plume salt balance is primarily between the cross-shore advection of fresh, riverine waters and vertical entrainment of salty waters from beneath the pycnocline. In the absence of ice, the nearshore circulation and mixing is controlled by the along-shore winds. These winds are particularly important in autumn for they control the sources of waters that prevail on the inner shelf throughout the landfast ice season.

The LIZs of arctic shelves are the Arctic Ocean's estuaries (Macdonald and Carmack, 1991; Macdonald and Yu, 2005), where river runoff and its terrestrial burdens are physically and biochemically transformed before entering the Arctic basin. These processes are intricately tied to the annual cycles of landfast ice and river discharge, both of which should change under a warming climate. Prominent amongst these changes will be an earlier spring break-up and a later fall freeze-up (George et al., 2004; Hutchings and Rigor, 2012; Yu et al., 2013; Mahoney et al., 2014). A shorter ice growth season will lead to thinner, mechanically weaker landfast ice and so alter ice deformation patterns. Warming will increase runoff and alter the seasonal phasing of river discharge. The spring freshet should occur earlier, persist longer, and comprise a smaller fraction of the annual discharge (and perhaps the dissolved and particulate riverine loads) because runoff will increase from summer through fall. Such changes will likely result in a reorganization of freshwater transport and stratification patterns, biogeochemical cycles, and sediment processing on the Arctic Ocean's inner shelves, and by extension the outer shelf and basin.

Author agreement/Declaration

We certify that all authors have seen and approved the submitted version of the manuscript. We warrant that the article represents the authors' original work and that this work has not been previously published nor is it under consideration for publication elsewhere. TW, SD, AM, and JT participated in the intellectual formulation of the paper, all authors participated in the writing, data collection and/or processing.

Acknowledgements

This research was supported by the Minerals Management Service (M03PC00015) (now the Bureau of Ocean Energy Management; BOEM) and the State of Alaska's Department of Environmental Conservation (ADEC). We are especially grateful to our program managers, Richard Prentki (BOEM) and Larry Dietrick (ADEC), for their dedication, encouragement, and assistance throughout the entire project. The measurements obtained in this study would not have been made without advice and enthusiasm of Erk Reimnitz and Humfrey Melling. David Leech was responsible for all phases of the mooring efforts. The divers, Melissa Deiman, Markus Janout, Sean Harper, and Caleb Conley assisted in mooring recoveries. We thank Billy Adams, Lee Kayoktuk, Ian Koyoktuk, Wilson Soplu, and Hugh Olemaun for performing the Kaktovik drifter deployments. Support for the drifters and their deployment was provided by BOEM and the North Slope Borough-Shell Baseline Studies Program. Liz Dobbins processed the drifter data. TW thanks David Heggie for his hospitality while preparing this manuscript. The mooring and CTD data are archived with BOEM and the authors. The drifter data are available at http://dm.sfos.uaf.edu/chukchi-beaufort/data/drifters/. Sea level data from Prudhoe Bay was downloaded from: https://tidesandcurrents.noaa.gov/stationhome.html?id=9497645. RADARSAT-1 data was obtained from the Alaska Satellite Facility, and MODIS imagery was retrieved from the Geographic Information Network of Alaska (GINA). None of the funders

participated in the study design; the collection, analysis and interpretation of data; in the writing of the report; and in the decision to submit the article for publication.

References

Aagaard, K., 1984. The beaufort undercurrent. In: Barnes, P.W., Schell, D.M., Reimnitz, E. (Eds.), The Alaskan Beaufort Sea: Ecosystems and Environment. Academic Press, New York, pp. 47–71.

Alkire, M., Trefry, J.H., 2006. Transport of spring floodwater from rivers under ice to the Alaskan Beaufort Sea. J. Geophys. Res. 111. http://dx.doi.org/10.1029/2005JC003446.

Barnes, P.W., Rearic, D.M., Reimnitz, E., 1984. Ice gouging characteristics and processes. In: Barnes, P.W., Schell, D.M., Reimnitz, E. (Eds.), The Alaskan Beaufort Sea: Ecosystems and Environment. Academic Press, New York, pp. 185–212.

Barnes, P.W., Reimnitz, E., Fox, D., 1982. Ice rafting of fine-grained sediment, a sorting and transport mechanism, Beaufort Sea, Alaska. J. Sediment. Petrol. 52 (2), 493–502.

Barrick, D., Lipa, B., 1986. Correcting for distorted antenna patterns in CODAR ocean surface measurements. IEEE J. Ocean. Eng. 11, 304–309.

Brower, W.A., Jr., Baldwin, R.G., C.N., Williams, Jr., Wise, J.L., Leslie, L.D., 1988. Climate atlas of the outer continental shelf waters and coastal regions of Alaska, volume III, Chukchi-Beaufort Sea, National Climatic Data Center, Asheville, NC, 28801, p. 497.

Brugler, E.T., Pickart, R.S., Moore, G.W.K., Roberts, S., Weingartner, T.J., Statscewich, Hank, 2014. Seasonal to interannual variability of the Pacific water boundary current in the Beaufort Sea. Progress. Oceanogr. 127, 1–20.

Davis, R.E., 1985. Drifter observations of coastal surface currents during CODE: the method and descriptive view. J. Geophys. Res. 90, 4741–4755.

Dean, K.G., Stringer, W., Ahlnaes, K., Searcy, S.C., Weingartner, T., 1994. The influence of river discharge on the thawing of sea ice: mackenzie River Delta: albedo and temperature analysis. Polar Res. 13, 83–94.

Denman, K.L., Miyake, M., 1973. Upper layer modification at ocean station Papa: observations and simulation. J. Phys. Oceanogr. 3, 185–196.

Divine, D.V., Korsnes, R., Makshtas, A.P., 2004. Temporal and spatial variation of shorefast ice in the Kara Sea. Cont. Shelf Res. 24, 1717–1736.

Dmitrenko, I.A., Tyshko, K.N., Kirillov, S.A., Eicken, H., Holemann, J.A., Kassens, H., 2005. Impact of flaw polynyas on the hydrography of the Laptev Sea. Glob. Planet. Change 48, 9–27.

Dunton, K., Schonberg, S.V., Cooper, L.W., 2012. The ecology of coastal waters and estuarine lagoons of the eastern Alaskan Beaufort Sea. Estuaries Coasts 35, 416–435.

Dunton, K.H., Weingartner, T., Carmack, E.C., 2006. The nearshore western Beaufort Sea ecosystem: circulation and importance of terrestrial carbon in arctic coastal food webs. Prog. Oceanogr. 71, 362–378.

Eicken, H., Ritchie, L.A., Barlau, A., 2011. The role of local and indigenous knowledge in arctic and offshore oil and gas development, environmental hazard mitigation, and emergency response. In: Lovecraft, A.L., Eicken, H. (Eds.), North by 2020: Perspectives on Alaska's Changing Socio-Economic Systems. University of Alaska Press, Fairbanks, Alaska, USA, pp. 577–604.

Eicken, H., Dmitrenko, I., Tyshko, K., Darovskikh, A., Dierking, W., Blahak, U., Groves, J., Kassens, H., 2005a. Zonation of the Laptev Sea landfast ice cover and its importance in a frozen estuary. Glob. Planet. Change 48, 55–83.

Eicken, H., Gradinger, R., Gaylord, A., Mahoney, A., Rigor, I., Melling, H., 2005b. Sediment transport by sea ice in the Chukchi and Beaufort Seas: Increasing importance due to changing ice conditions? Deep-SeaResearch II 52, 3281–3302.

George, J.C., Huntington, H.P., Brewster, K., Eicken, H., Norton, D.W., Glenn, R., 2004. Observations on shorefast ice dynamics in. Arct. Alsk. Responses Iñupiat Hunt. Community Arct. 57, 363–374.

Guay, C., Falkner, K.K., 1998. A survey of dissolved barium in the estuaries of major Arctic rivers and adjacent seas. Cont. Shelf Res. 8, 859–882.

Hutchings, J.K., Rigor, I., 2012. Role of ice dynamics in anomalous conditions in the Beaufort Sea during 2006 and 2007. J. Geophys. Res. 117, C00e04. http://dx.doi.org/10.1029/2011JC007182.

Itkin, P., Losch, M., Gerdes, R., 2015. Landfast ice affects the stability of the Arctic halocline: evidence from a numerical model. J. Geophys. Res. 120, 2622–2635. http://dx.doi.org/10.1002/2014JC010353.

Kasper, J., Weingartner, T., 2015. The spreading of a buoyant plume beneath a landfast ice cover. J. Phys. Oceanogr. 45, 478–494.

Kasper, J.L., Weingartner, T.J., 2012. Modeling winter circulation under landfast ice: the interaction of winds with landfast ice. J. Geophys. Res. 117, C04006. http://dx.doi.org/10.1029/2011JC007649.

Kohut, J., Glenn, S.M., 2003. Improving HF radar surface current measurements with measured antenna beam patterns. J. Atmos. Ocean. Technol. 1303–1316.

Lemieux, J.-F., Tremblay, L.B., Dupont, F., Plante, M., Smith, G.C., Dumont, D., 2015. A basal stress parameterization for modeling landfast ice. J. Geophys. Res. 120, 3157–3173. http://dx.doi.org/10.1002/2014JC010678.

Lentz, S.J., 1995. Sensitivity of the inner shelf circulation to the form of the eddy viscosity profile. J. Phys. Oceanogr. 25, 19–28.

Li, Z., Weisberg, R.H., 1999. Florida continental shelf response to upwelling favorable wind forcing 2. Dyn. J. Geophys. Res. 104, 23427–23442.

Lu, P., Li, Z., Cheng, B., Leppäranta, M., 2011. A parameterization of the ice-ocean drag coefficient. J. Geophys. Res. 116, C07019. http://dx.doi.org/10.1029/2010JC006878m.

Macdonald, R.W., Yu, Y., 2005. The mackenzie estuary of the arctic ocean. In: Wangersky, P.J. (Ed.), Handbook of Environmental Chemistry 5/H. Springer-Verlag, Berlin, pp. 91–120.

Macdonald, R.W., Carmack, E.C., 1991. The role of large-scale under-ice topography in separating estuary and ocean on an arctic shelf. Atmos.-Ocean 29, 37–51.

Macdonald, R.W., Carmack, E.C., McLaughlin, F.A., Falkner, K.K., Swift, J.H., 1999. Connections among ice, runoff, and atmospheric forcing in the Beaufort Gyre. Geophys. Res. Lett. 26 (15), 2223–2226.

Macdonald, R.W., Paten, D.W., Carmack, E.C., Omstedt, A., 1995. The freshwater budget and under-ice spreading of Mackenzie River water in the Canadian Beaufort Sea based on salinity and measurements in water and ice. J. Geophys. Res. 100 (C1), 895–919.

Mahoney, A., Eicken, H., Gaylord, A., Gens, R., 2014. Alaskan landfast sea ice: links with bathymetry and atmospheric circulation. Cold Reg. Sci. Technol. 103, 41–56.

Mahoney, A., Eicken, H., Shapiro, L., Gaylord, A., 2007a. Alaskan landfast sea ice: links with bathymetry and atmospheric circulation. J. Geophys. Res. 112, C02001. http://dx.doi.org/10.1029/2006JC003559.

Mahoney, A., Eicken, H., Shapiro, L., 2007b. How fast is landfast sea ice? A study of the attachment and detachment of nearshore ice at Barrow, Alaska. Cold Reg. Sci. Technol. 47, 233–255.

Matthews, J.B., 1981. Observations of under-ice circulation in a shallow lagoon in the Alaskan Beaufort Sea. Ocean Manag. 6, 223–234.

McClelland, J.W., Holmes, R.M., Dunton, K.H., Macdonald, R.W., 2012. The Arctic Ocean Estuary. Estuaries Coasts 35, 353–368.

McPhee, M.G., 1990. Small-scale processes. In: Smith Jr.W.O. (Ed.), Polar Oceanography Part A: Physical Science. Academic Press, New York (287–280).

McPhee, M., Kottmeier, G.C., Morison, J.H., 1999. Ocean het flux in the central Weddell Sea during winter. J. Phys. Oceanogr. 29, 1166–1179.

Melling, H., 1993. The formation of a haline shelf front in a ice-covered arctic sea. Cont. Shelf Res. 13, 1123–1147.

Mesinger, F., et al., 2006. North American Regional Re-analysis 87. Bulletin of the American Meteorological Society, pp. 343–360.

Morris, K., Li, S., Jefferies, M., 1997. Meso- and microscale sea-ice motion in the East Siberian Sea as determined from ERS-1 SAR data. J. Glaciol. 45 (15), 370–383.

Ohshima, K.I., 2000. Effect of landfast sea ice on coastal currents driven by the wind. J. Geophys. Res. 105 (C7), 17133–17141.

Overland, J.E., Pease, C.H., 1984. Wind-driven ice drift in a shallow sea. J. Geophys. Res. 90 (C4), 6525–6531.

Potter, R.A., Weingartner, T.J., 2010. Surface circulation radar mapping in Alaskan coastal waters: Beaufort Sea and Cook Inlet. Final Report to the Minerals Management Service (now BOEM). MMS Contract No.1435-01-04-CT-35579, M04PC00002 and M08PC20006, p. 144.

Reimnitz, E., 2000. Interaction of river discharge with sea ice in proximity of Arctic deltas: a review. Polarforschung 70, 123–134.

Reimnitz, E., Kempema, E.W., Weber, W.S., Clayton, J.R., Payne, J.R., 1990. Suspended-matter scavenging by rising frazil ice. In: Ackley, S.F., Weeks, W.F. (Eds.), Sea Ice Properties and Processes: Proceedings of the W. F. Weeks Sea Ice Symposium, 97–100. Cold Regions Research and Engineering Laboratory Monograph, no 90-1. U.S. Army Cold Regions Research and Engineering Laboratory.

Reimnitz, E., Kempema, E.W., 1984. Pack ice interaction with stamukhi shoal. In: Barnes, P.W., Schell, D.M., Reimnitz, E. (Eds.), The Alaskan Beaufort Sea: Ecosystems and Environment. Academic Press, New York, pp. 159–184.

Rember, R.D., Trefry, J.H., 2004. Increased concentrations of dissolved trace metals and organic carbon during snowmelt in rivers of the Alaskan Arctic. Geochim. Et. Cosmochim. Acta 68 (3), 477–489. http://dx.doi.org/10.1016/S0016-7037(03)00458-7.

Searcy, C., Dean, K., Stringer, W., 1996. A river-coastal sea ice interaction model: Mackenzie River Delta. J. Geophys. Res. 101, 8885–8894.

Schulze, L.M., Pickart, R.S., 2012. Seasonal variation of upwelling in the Alaskan Beaufort Sea: impact of sea ice cover. J. Geophys. Res. 117, C06022. http://dx.doi.org/10.1029/2012JC007985.

Shaw, W.J., Stanton, T.P., McPhee, M.G., Kikuchi, T., 2008. Estimates of surface roughness length in heterogeneous under-ice boundary layers. J. Geophys. Res. 113 (C08030). http://dx.doi.org/10.1029/2007. (JC004550).

Shirasawa, K., Ingram, R.G., 1997. Currents and turbulent fluxes under first-year sea ice Resolute Passage, Northwest Territories, Canada. J. Mar. Syst. 11, 21–32.

Stierle, A.P., Eicken, H., 2002. Sediment inclusions in Alaskan Coastal Sea Ice: spatial distribution, interannual variability, and entrainment requirements. Arct. Antarct., Alp. Res. 34 (4), 465–476.

Trefry, J.H., Trocine, R.P., Alkire, M.B., Semmler, C.M., Savoie, M., Rember, R.D., 2009. cANIMIDA Tasks 3 and 4: Sources, Concentrations, Composition, Partitioning and Dispersal Pathways for Suspended Sediments and Potential Metal Contaminants in the Coastal Beaufort Sea. Final Report. U.S. Department of Interior, Minerals Management Service, Anchorage, Alaska, pp. 2009–2014.

Tucker III, W.B., Weeks, W.F., Frank, M., 1979. Sea Ice ridging over the Alaskan continental shelf. J. Geophys. Res. 84, 4885–4897.

Wadhams, P., 1986. The seasonal ice zone. In: Untersteiner, N. (Ed.), TheGeophysics of Sea Ice. Plenum Press, New York, pp. 825–991.

Weingartner, T.J., Danielson, S.L., Okkonen, S.R., 2009. Circulation and Water Property Variations in the Nearshore Alaskan Beaufort Sea, Final Report. U.S. Department of Interior, Minerals Management Service, Anchorage, Alaska, pp. 103 OCS Study MMS 2005-028.

Volkov, V., Johannessen, O., Borodachev, V., Voinov, G., Pettersson, L., Bobylev, L., Kouraev, A., 2002. In: Volkov, V.A., Johannessen, O.M., Borodachev, V.E. (Eds.), Polar Seas Oceanography. An Integrated Case Study of the Kara Sea. Springer, London, pp. 450.

Yu, Y., Stern, H., Fowler, C., Fetterer, F., Maslanik, J., 2013. Interannual variability of arctic landfast ice between 1976 and 2007. J. Clim(http://journals.ametsoc.org/doi/abs/10.1175/JCLI-D-13-00178.1).

Zubov, N.H., 1945. L'dy Arktiki (arctic ice). Izdatel'stvo Glavsevmorputi, Moscow, (U.S. Navy hydrographic Office, Translation 217, 1963; available as AD426971 from NTIS, Springfield, VA.), p. 360.